Design and Fabrication of a Supporting Structure for 3.6 m Long Nb_3Sn Racetrack Coils

P. Ferracin, G. Ambrosio, M. Anerella, E. Barzi, S. Caspi, D. W. Cheng, D. R. Dietderich, S. A. Gourlay, A. R. Hafalia, C. R. Hannaford, A. F. Lietzke, A. R. Nobrega, G. L. Sabbi, J. Schmalzle, P. J. Wanderer, and A. V. Zlobin

***Abstract*—As part of the LHC Accelerator Research Program (LARP), three US national laboratories (BNL, FNAL, and LBNL) are currently engaged in the development of superconducting magnets for the LHC Interaction Regions (IR) beyond the current design. As a first step towards the development of long Nb_3Sn quadrupole magnets, a 3.6 m long structure, based on the LBNL Subscale Common-Coil Magnet design, will be fabricated, assembled, and tested with aluminum-plate "dummy coils". The structure features an aluminum shell pre-tensioned over iron yokes using pressurized bladders and locking keys (bladder and key technology). Pre-load homogeneity and mechanical responses are monitored with pressure sensitive films and strain gauges mounted on the aluminum shell and the dummy coils. The details of the design and fabrication are presented and discussed, and the expected mechanical behavior is analysed with finite element models.**

***Index Terms*—LARP, Nb_3Sn, superconducting magnets.**

I. Introduction

THE LHC Accelerator Research Program (LARP) is developing Nb_3Sn quadrupole magnet models for a luminosity upgrade of the Large Hadron Collider (LHC) [1]. A major milestone in this development includes the assembly and test of 4 m long quadrupole cold masses. These quadrupole magnets will be the first Nb_3Sn accelerator magnet models significantly longer than 1 m, and they will approach the length of a real accelerator magnet [2]. In order to provide a reliable test bed for the fabrication and test of long Nb_3Sn coils, LARP has started the development of the long racetrack magnet LRS01 [3]. The magnet will feature two 3.6 m long racetrack coils [4], contained in a supporting structure based on an aluminum shell pre-tensioned with bladders [5]. As a first step of the magnet development, a preliminary assembly and test of the support structure with "dummy coils" made of aluminum plates will be conducted. The test will provide an early feed-back in terms of assembly procedure, loading operation, and stress homogeneity.

Manuscript received August 26, 2006. This work was supported by the Director, Office of Energy Research, Office of High Energy and Nuclear Physics, High Energy Physics Division, U.S. Department of Energy, under Contract No. DE-AC02-05CH11231.

P. Ferracin, S. Caspi, D. W. Cheng, D. R. Dietderich, S. A. Gourlay, A. R. Hafalia, C. R. Hannaford, A. F. Lietzke, and G. L. Sabbi are with Lawrence Berkeley National Lab, Berkeley, CA 94720 USA (e-mail: pferracin@lbl.gov).

G. Ambrosio, E. Barzi, A. R. Nobrega and A. V. Zlobin are with Fermilab National Accelerator Laboratory, Batavia, IL 60510 USA.

M. Anerella, J. Schmalzle, and P. J. Wanderer are with Brookhaven National Laboratory, Upton, NY 11973-5000 USA.

Digital Object Identifier 10.1109/TASC.2007.898509

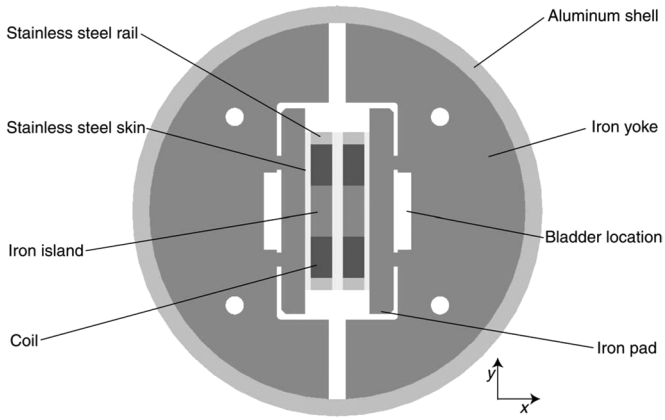

Fig. 1. Cross-section of the long racetrack magnet.

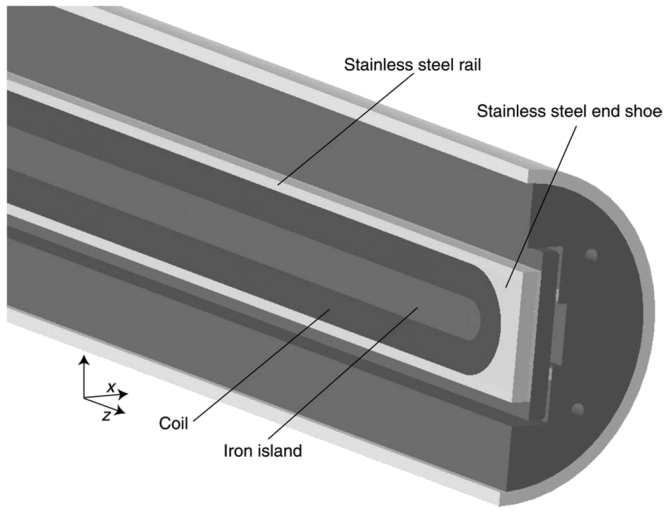

Fig. 2. 3D geometry of the long racetrack magnet.

We present in this paper the main parameters of the LRS01, with an analysis of the mechanical behavior from assembly to excitation. The development of the support structure is then described, pointing out the issues related to fabrication and assembly, and introducing the plan for the test with dummy coils.

II. Magnet Design and Parameters

The design of LRS01 is based on the lay-out of the Subscale Common-Coil Magnets (SM) developed at LBNL [6]. The cross-section is depicted in Fig. 1, whereas the details of the end region are shown in Fig. 2. Two double-layer racetrack coil modules (with 21 turns per layer) are wound around iron

TABLE I
MAGNET PARAMETERS

	Unit	
Number of turns per layer		21
Strand diameter	mm	0.700
Number of strands		20
Cable width (bare)	mm	7.793
Cable thickness (bare)	mm	1.275
Insulation thickness	mm	0.092
Cu/Sc ratio		0.90
J_c(12 T,4.2 K)	A/mm^2	2800
B_{peak}(4.2 K)	T	12.23
I_{ss} (4.2 K)	kA	10.80
I_{ss} (4.2 K) per strand	A	540
Inductance @ I_{ss} (4.2 K)	mH/m	1.5
Energy @ I_{ss} (4.2 K)	kJ/m	86
F_x per quadrant @ I_{ss}	kN/m	+1903
F_y per quadrant @ I_{ss}	kN/m	-9
F_z per quadrant @ I_{ss}	kN	20

islands and contained within end shoes, rails, and skins. The coil modules are then connected in a common-coil configuration and held together by two bolted iron pads, which provide initial pre-stress and alignment. This coil-pack subassembly is inserted in the shell/yoke subassembly, consisting of iron yoke laminations and an aluminum shell. The 12.7 mm-thick shell has an outer diameter of 305 mm. A gap between pad and yoke provide room for inserting high-pressure bladders. Pressurizing the bladders spreads the pad and yoke apart, enlarging the gap and allowing the insertion of four symmetrically located keys. During bladder pressurization, the shell deformation is monitored with strain gauges. Once the target strain is attained, the keys are inserted, and the bladders are deflated and removed, thus allowing the shell-yoke structure to collapse on the keys, and pre-load the coil-pack. During cool-down, the shell generates additional pre-load on the coil-pack, as a result of the different thermal contraction of aluminum and iron.

With respect to the original length of the SM structure (about 300 mm long), the scale-up of the supporting structure to a total length of 3.6 m required a few modifications. In particular, key-ways have been included in the yoke design (see "Bladder location" in Fig. 1) to facilitate bladder insertion and removal with thicker pulling shims. Consequently, the ID of the aluminum shell has been increased by about 60 mm. The magnet's parameters are given in Table I: the short sample computations have been performed assuming a J_c in the superconductor of 2800 A/mm^2 at 4.2 K and 12 T.

III. MAGNETIC ANALYSIS

The peak field of the magnet is located in the coil inner layer. If we consider a path moving from the innermost turn (close to the island) to the outermost turn (close to the rail), as shown in the inset picture of Fig. 3, the highest field of 12.23 T is reached approximately between turn 10 and turn 12 (counting from the island).

A 3D magnetic analysis indicated that the field in the coil significantly decreases in the end region. By moving along turn 11 from the center of the magnet towards the end (see path depicted in the inset picture of Fig. 4), one can notice that the field starts

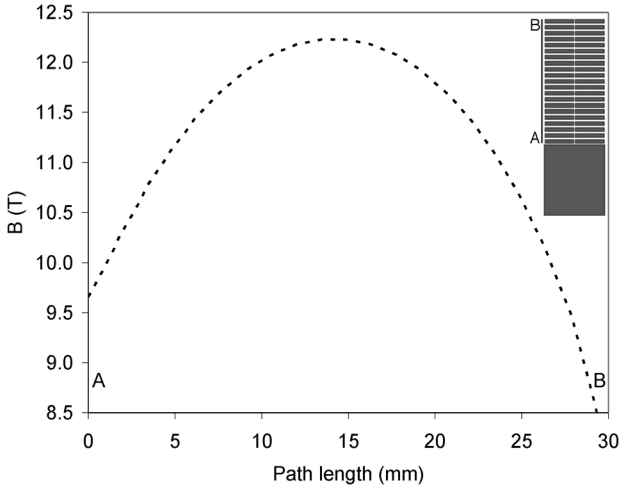

Fig. 3. Magnetic field (T) along a path moving from the innermost to the outermost turn on the inner layer.

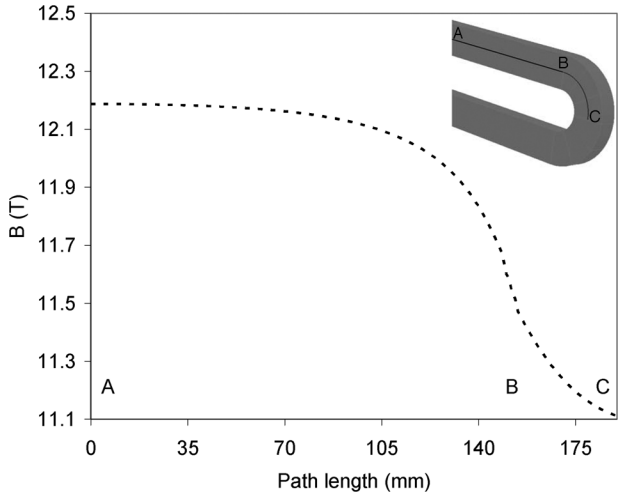

Fig. 4. Magnetic field (T) along a path moving from the center to end of the inner layer.

decreasing at approximately 105 mm from the end of the straight section (location A). In the end region, the field varies from a maximum of 11.60 T (location B) to a minimum of 11.00 T (location C).

IV. MECHANICAL ANALYSIS

A finite element mechanical analysis was performed to analyze structural issues of LRS01. A 2D model was used to compute shell and coil stresses in nominal conditions and to evaluate the effect of fabrication tolerances on the loads acting on the components. A 3D analysis was then focused on the impact of Lorentz force on the coil-island contact region, and on the relative sliding between shell and yoke during cool-down.

A. Shell and Coil Stress

In a common-coil configuration, the largest component of the magnetic force tries to separate the two coil modules along the horizontal direction, and only a small force is acting in the vertical direction (see Table I). In order to withstand the horizontal electromagnetic force and limit coil motion during excitation, we plan to pre-tension the shell at room temperature

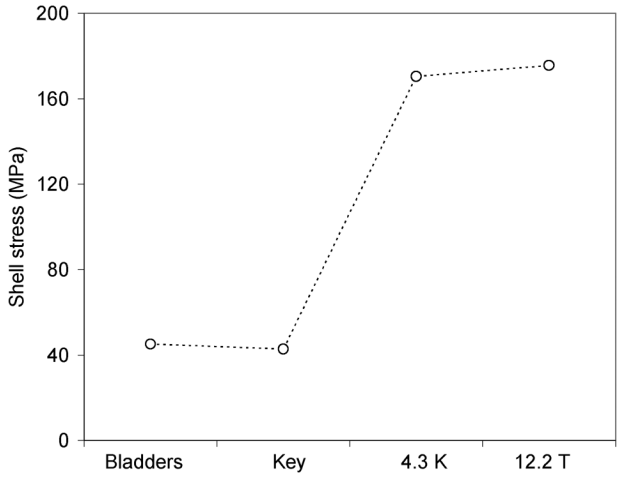

Fig. 5. Computed shell stress during assembly, cool-down, and excitation.

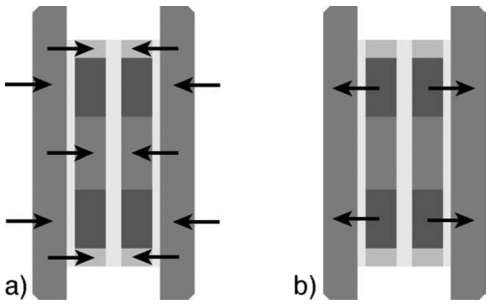

Fig. 6. Direction of the compressive forces from the structure to the coil module after cool-down (a); direction of the main Lorentz force component during excitation (b).

to the nominal stress of 45 MPa (see Fig. 5). After cool-down, the shell tension is expected to increase up to 180 MPa. This level of stress corresponds to a total horizontal compressing force on the coil-pad subassembly of 2200 kN/m (about 10% higher than the horizontal Lorentz force). Nevertheless, because of the differences in thermal contraction among the coil module components, the force produced by the shell is mainly transmitted to the iron island and the stainless steel rails (Fig. 6(a)), both characterized by a thermal contraction lower than that of the coil. As a result, the pads are pushed against island and rails, and, consequently, the coil stress safely remains below 40 MPa during assembly and after cool-down (Fig. 7). When the magnet is energized, the Lorentz forces, mainly directed outwardly in the horizontal direction (Fig. 6(b)), tend to move the two coil modules apart, at the same time compressing the coil blocks against the pads. The resulting compressive stress on the conductor is therefore about 75 MPa on the pad side, with complete unloading of the side facing the other coil (Fig. 7).

B. Tolerance Analysis

As already mentioned in Section II, bladders are inflated in between yoke and pads during the room temperature loading operation. The resulting pressure compresses the pad against the coil and the yoke against the shell, at the same time widening the gap between the two subassemblies. This increase of gap width produced by the bladders is called the "interference gap".

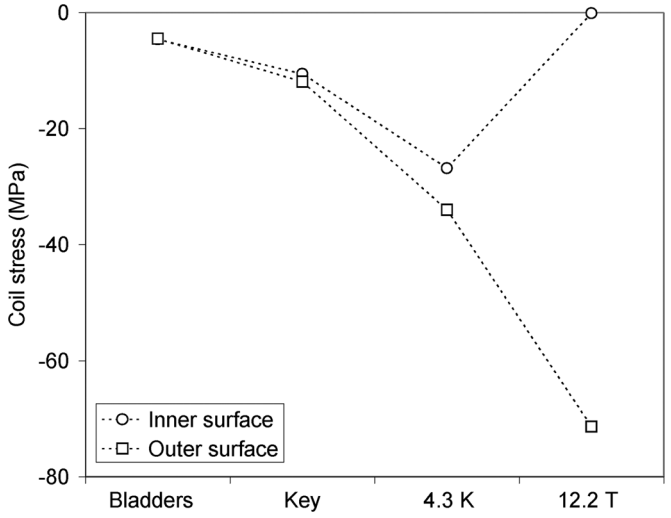

Fig. 7. Average computed coil horizontal stress on the inner (facing the other coil) and the outer surface (facing the pad) during magnet operations.

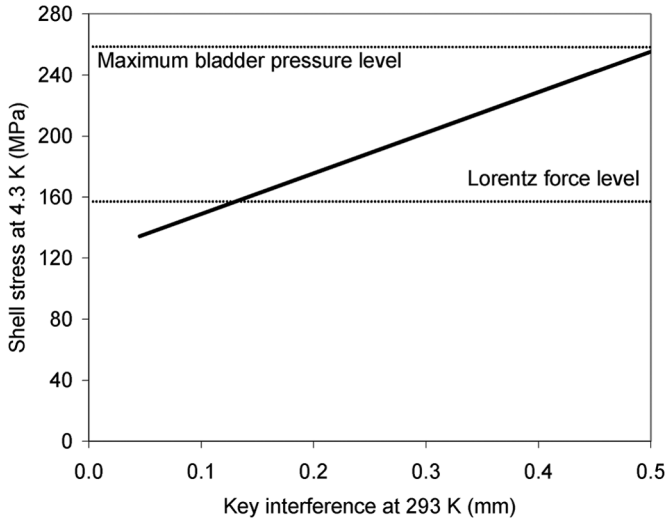

Fig. 8. Computed shell tension as a function of the key interference at the end of the assembly.

Once the target tension in the shell is achieved, the resulting interference gap is locked-in by shimmed keys. Then, the bladders are deflated. It is therefore possible to plot the stress in the shell after cool-down, as a function of the key interference. For example, as shown in Fig. 8 (solid line), in order to reach a shell tension of 180 MPa at 4.3 K, the bladders have to create a pad-yoke interference at room temperature of about 0.2 mm. In the same plot, two critical shell stress levels (dashed lines) are depicted. The lower level corresponds to the shell stress that produces a horizontal force on the coil pack equal to the Lorentz force. The upper level indicates the maximum shell stress that can be reached after cool-down, assuming bladder pressure and component stress within the maximum limits (with a safety margin). These two values define a lower and an upper bound for the shell tension at 4.3 K, so that 1) the coil motions during excitation are minimized, and 2) the component stresses are maintained within acceptable levels.

In addition, the dependence of the shell tension on the interference can be used to evaluate the impact of the tolerances of

fabrication. In fact, to a certain extent, a variation of a component dimension with respect to the design values will produce the same effect as an equivalent variation of the interference. By adding all the tolerances of fabrication for shell, yoke, and pad, one obtains a total range of variation for the structure dimensions of ± 0.2 mm. This variation is consistent with the results of Fig. 8, where we showed that, within an interference range of approximately 0.4 mm, the stresses of the structure remains within acceptable levels.

C. 3D Effects

A 3D finite element model was used to address mechanical issues related to end regions and axial effects. Similar analyses were performed on other LARP magnets [7]. We focused on the effect of axial Lorentz forces on the contact region between the innermost turn and the iron island. Under the assumption that the coil has an integrated thermal contraction in the z direction of 2.7×10^{-3} (compared with 2.0×10^{-3} for the iron island), the conductor is expected to undergo axial tension after cool-down, with a consequent longitudinal compression of the island. According to the model predictions, the resulting contact force overcomes the axial Lorentz force (which tends to push the coil outwards in the longitudinal direction), and prevents the development of gaps between pole turn and island in the end region.

The analysis of the interaction between shell and yoke provided different results depending on the friction coefficient assumed in the computations. If frictionless contact is considered between yoke and shell, we expect after cool-down a relative displacement of the shell with respect to the yoke of about 5.6 mm at both ends. Such a sliding action is produced by the differential thermal contraction between aluminum and iron, and by the Poisson's effect of the azimuthal shell tension along the longitudinal direction. If a friction factor of 0.2 is assumed, the computed relative sliding is reduced to 1.5 mm.

V. Fabrication of the Supporting Structure

At the time of submission of this paper, all the components of the supporting structure have been fabricated and delivered to LBNL. Several options were considered for machining the aluminum shell: from boring out a solid round to size, to coring a rod in order to minimize the amount of wasted material. Due to difficulties in handling long and solid materials, it was decided to start with a thick-walled aluminum tube, and then bore and hone its ID to size. The 50 mm-thick yoke laminations were conventionally machined, turned on a lathe, and split in half. The final profile was CNC (Computer Numerically Controlled) machined. The dummy coils were made out of aluminum and milled to the desired thickness.

VI. Next Step: Instrumentation, Assembly and Test

As future steps, the development of the structure will include instrumentation, assembly, and cool-down test with dummy coils. Strain gauges will be installed at 6 different axial locations along the shell to investigate possible non-homogeneities of the azimuthal and longitudinal stress. The same gauge configuration will be mounted on the dummy coils. The pads and dummy coils will be pre-assembled as a subassembly. The yoke laminations will also be pre-assembled with tie rods as subassembly-halves, and inserted in the shell. These operations required the design and fabrication of special tooling and fixtures (see Fig. 9): in particular, an 8 m long assembly beam, equipped with hydraulic pistons, will be utilized to slide the first stack of yoke laminations inside the shell. Then, after a 180° rotation of this first yoke-half subassembly performed with a system of rafts and cradles, the dummy coils, the pads, and the second stack of yoke laminations will be slid in. After final assembly and bladder and key preloading, the structure will undergo cool-down.

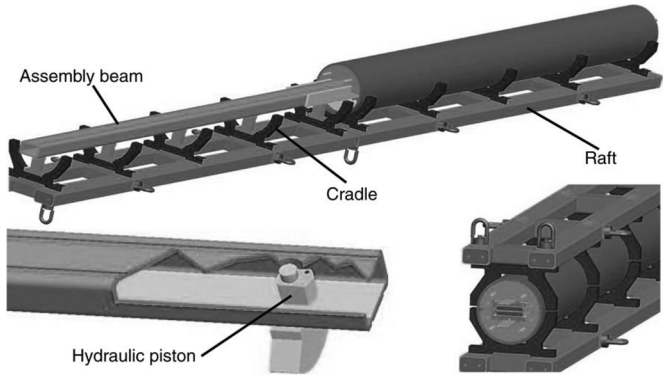

Fig. 9. Assembly tooling and fixtures.

VII. Conclusions

The design and analysis of the long racetrack magnet LRS01 has been presented. The magnet has an expected peak field of 12.23 T, with about 1 T of margin in the ends. A mechanical analysis of the support structure indicated that the shell provides the required pre-load minimizing the stress in the coils. No significant conductor motions are expected in the ends during magnet excitation. The structure will initially be assembled, loaded, and cooled down with dummy coils. The test will provide useful information towards the final assembly of the LRS01 magnet with 3.6 m long Nb_3Sn coils.

References

[1] S. A. Gourlay *et al.*, "Magnet R&D for the IS LHC accelerator research program," *IEEE Trans. Appl. Supercond.*, vol. 16, no. 2, pp. 324–327, June 2006.

[2] G. Ambrosio *et al.*, "Design of Nb_3Sn coils for LARP long magnets," presented at the Applied Superconductivity Conference 2006, Seattle, WA, USA, August 29–September 1, 2006.

[3] G. Ambrosio *et al.*, "Design of the first LARP long racetrack magnet," LARP-SRD-02, November 2006.

[4] P. J. Wanderer *et al.*, "LARP long Nb_3Sn racetrack coil program," presented at the Applied Superconductivity Conference 2006, Seattle, WA, USA, August 29–September 1, 2006.

[5] S. Caspi *et al.*, "The use of pressurized bladders for stress control of superconducting magnets," *IEEE Trans. Appl. Supercond.*, vol. 11, no. 1, pp. 2272–2275, March 2001.

[6] A. R. Hafalia *et al.*, "An approach for faster high field magnet technology development," *IEEE Trans. Appl. Supercond.*, vol. 13, no. 2, pp. 1258–1261, June 2003.

[7] S. Caspi *et al.*, "Design and analysis of TQS01, a 90 mm Nb_3Sn model quadrupole for the LHC luminosity upgrade based on a key and bladder assembly," *IEEE Trans. Appl. Supercond.*, vol. 16, no. 2, pp. 358–361, June 2006.